Advances in Materials Technology for Fossil Power Plants
Proceedings from the Eighth International Conference
October 11–14, 2016, Albufeira, Algarve, Portugal
https://doi.org/10.31399/asm.cp.am-epri-2016p0318

DEVELOPMENT OF HIGH CR CONTAINING FECRAL ALLOYS FOR FOSSIL ENERGY STRUCTURAL APPLICATIONS

Yukinori Yamamoto, Bruce A. Pint
Oak Ridge National Laboratory, Oak Ridge, TN, USA

Benjamin Shassere, Sudarsanam Suresh Babu
The University of Tennessee, Knoxville, TN, USA

ABSTRACT

New Fe-base ferritic alloys based on Fe-30Cr-3Al-Nb-Si (wt.%) were proposed with alloy design concepts and strategies targeted at improved performance of tensile and creep-rupture properties, environmental compatibilities, and weldability, compared to Grade 91/92 type ferritic-martensitic steels. The alloys were designed to incorporate corrosion and oxidation resistance from high Cr and Al additions and precipitate strengthening via second-phase intermetallic precipitates (Fe_2Nb Laves phase), with guidance from computational thermodynamics. The effects of alloying additions, such as Nb, Zr, Mo, W, and Ti, on the properties were investigated. The alloys with more than 1 wt.% Nb addition showed improved tensile properties compared to Gr 91/92 steels in a temperature range from 600-800°C, and excellent steam oxidation at 800°C as well. Creep-rupture properties of the 2Nb-containing alloys at 700°C were comparable to Gr 92 steel. The alloy with a combined addition of Al and Nb exhibited improved ash-corrosion resistance at 700°C. Additions of W and Mo were found to refine the Laves phase particles, although they also promoted the coarsening of the particle size during aging. The Ti addition was found to reduce the precipitate denuded zone along the grain boundary and the precipitate coarsening kinetics.

KEYWORDS: ferritic steel, Laves phase, tensile, creep, oxidation, and corrosion

INTRODUCTION

Traditional creep strength enhanced ferritic (CSEF) steels, such as ferritic-martensitic (FM) steels containing 9-12 wt% Cr, are now extensively used in coal-fired boilers, heat-recovery steam generators, and steam piping systems in fossil-fired power plants because of their excellent creep properties up to 600 - 620 °C matched with reasonable material costs [1,2]. However, CSEF steel weldments suffer from premature failures due to Type IV failures at the fine-grained heat affected zone (FGHAZ) [3-6]. Formation of the FGHAZ is attributed to α' to γ reverse transformation in the base metal adjacent to the weld due to heating above A_{c3} [7-9], indicating that the formation of weakened microstructure consisting of fine grains cannot completely be eliminated in traditional FM steel weldments [10]. In order to avoid such creep property degradation at the FGHAZ, another approach to develop a new, fully ferritic steel alloy is proposed. The class of alloys is essentially free from Type IV failure because α-γ phase transformation is not involved during the microstructure evolution. Several research groups are currently working actively to develop such class of steel alloys. Toda et al. [11] reported Fe-15Cr base ferritic steels, strengthened by stable Fe_2W type Laves phase precipitates, which exhibited two orders of magnitude longer creep life than Grade 92 steels at a given creep test condition. Kuhn et al. [12] reported Fe-(18-22)Cr High Performance Ferritic (HiPerFer) steels strengthened by $(Fe,Cr,Si)_2(Nb,W)$ Laves-phase precipitates which showed a good combination of the creep strength and the oxidation resistance.

Compared to traditional FM steels, the reduced microstructural instability in the ferritic alloys may enable an increase in the upper limit temperature. However, it also raises requirements in the alloy design that should incorporate the improved environmental compatibility in more aggressive corrosive/oxidized environments at elevated service temperatures. Based on this consideration, the present authors proposed a new alloy design with a base alloy composition of Fe-30Cr-3Al-0.2Si-(0-2)Nb in weight percent [13]. Better oxidation and corrosion resistance are expected by the combination of high Cr + Al + Nb contents based on previous alumina-forming austenitic stainless steel development [14], and the improved creep performance is expected via precipitate strengthening with Fe_2Nb Laves phase precipitates.

The objective of this paper is to discuss alloying effects of various properties in newly proposed, high Cr containing FeCrAl alloys, including tensile, creep, steam oxidation, and ash corrosion. Microstructure characterization was conducted to evaluate the effect of minor alloying additions on the second-phase precipitate kinetics. Thermal stability of the precipitates is also discussed.

EXPERIMENTAL PROCEDURES

Fe-30Cr-Al-Nb-Si base alloys, in wt.%, with minor alloying additions (0.1Zr, 2W, 1.5Mo, and 1Ti) were prepared in this study. A computational thermodynamics tool (JMatPro v.8 with Fe database) was used to guide the alloy composition range and the solution heat treatment temperatures. The bar-shape ingots were prepared by arc-melting and drop-casting. The analyzed alloy compositions are summarized in Table 1. The alloys were homogenized at 1300ºC in Ar gas atmosphere, and then thermo-mechanically treated in a temperature range of 1100 to 1300ºC to make plate samples with a recrystallized grain structure. The dog-bone shape tensile specimens (gage: 0.75mm t x 1.5mm w x 7.5mm l), creep specimens (gage: 0.75mm t x 3.2mm w x 13 mm l), oxidation test coupons (1mm x 10mm x 20mm), and the corrosion test specimens (6 mm dia. x 25mm length) were machined from the plate samples. Tensile tests were conducted from room temperature to 836ºC in laboratory air. The cyclic oxidation test was conducted at 800ºC in 10% water vapor. The ash-corrosion test was conducted by immersing the specimens into a mixed ash consisting of $30\%Fe_2O_3$-$30\%Al_2O_3$-$30\%SiO_2$-$5\%Na_2SO_4$-$5\%K_2SO_4$ and exposing in a mixed gas of $61\%CO_2$-$30\%H_2O$-$3\%O_2$-$0.45\%SO_2$ at 700°C for 500h. Metal loss was quantified by measuring the remaining metal radii through the cross-sectional observation of the tested specimens. The creep-rupture test was conducted at 700ºC and 70MPa in laboratory air. The aging study was conducted at 700°C for several periods of time up to 3000h. The microstructure of selected specimens was characterized by using scanning electron microscopy (SEM) and transmission electron microscopy (TEM).

*Table 1: Analyzed compositions of the alloy studied**

Alloy	Nominal	Fe.	Cr	Al	Nb	Si	Zr	W	Mo	Ti
A	3Al-0Nb	Bal.	30.23	2.91	-	0.19	-	-	-	-
B	3Al-1Nb	Bal.	29.97	2.93	0.99	0.19	-	-	-	-
BZ	3Al-1Nb-0.1Zr	Bal.	30.21	2.96	0.96	0.20	0.09	-	-	-
C	3Al-2Nb	Bal.	30.05	2.87	1.94	0.18	-	-	-	-
CZ	3Al-2Nb-0.1Zr	Bal.	30.10	2.97	1.99	0.18	0.09	-	-	-
D	1Al-2Nb-0.1Zr	Bal.	30.31	1.90	1.93	0.14	0.08	-	-	-
E	2Al-2Nb-0.1Zr	Bal.	30.10	0.94	1.98	0.18	0.06	-	-	-
BW	3Al-1Nb-2W	Bal.	30.15	2.90	1.05	0.16	-	1.96	-	-
BM	3Al-1Nb-1.5Mo	Bal.	29.89	2.91	0.97	0.21	-	0.05	1.48	-
BT	3Al-1Nb-1Ti	Bal.	29.96	2.90	0.98	0.19	-	-	-	0.98

*C < 50wppm, N < 47wppm, O < 40wppm, and S < 30wppm.

RESULTS AND DISCUSSION

Property Evaluations

The Fe-30Cr-3Al base alloys exhibited good high-temperature tensile properties comparable or even superior to Grade 91/92 steels, as shown in Fig. 1. Alloy A with 0Nb showed almost the same temperature dependence of the yield strength as Grade 91/92 steels. Alloy B with 1Nb, on the other hand, exhibited better yield strength than that of Grade 91/92 steels above ~600ºC, indicating a potential advantage of the Nb additions on improving mechanical properties at elevated temperatures. No significant degradation of the ductility in alloys A and B was observed from room temperature to above 800ºC, despite the elevated Cr contents over the Gr 91/92 steels. The addition of 0.1Zr (alloy BZ) to alloy B did not show any improvement in the yield strength, but exhibited a poor room temperature ductility lower than the others, suggesting no beneficial effect on the properties.

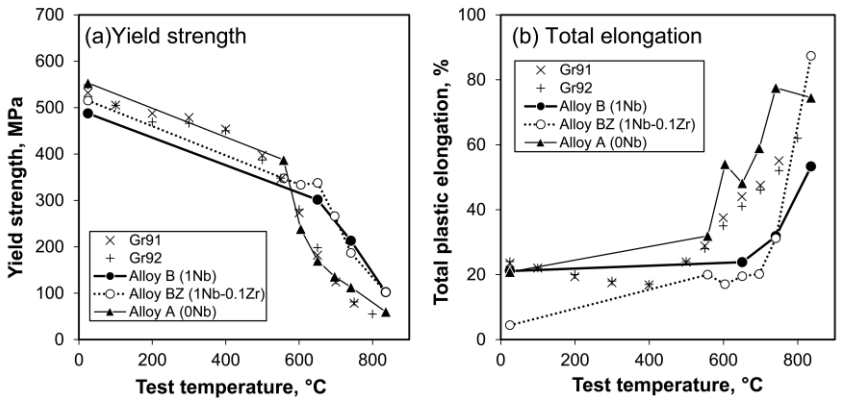

Figure 1: Tensile properties of Fe-30Cr-3Al base alloys, compared with Grade 91/92 steels (from NIMS creep data sheet, http://smds.nims.go.jp/creep/index_en.html)

Oxidation test result suggests that the combination of high Cr, Al, and Nb is the key to obtain better oxidation resistance, as shown in Fig. 2. The binary Fe-30Cr alloy (a reference material) showed significant weight loss after only 300h testing because of a formation and spallation of non-protective Fe-rich oxide nodules. Alloy A with 0Nb showed relatively slow weight loss which could potentially be due to volatilization of the oxide scale. On the other hand, the addition of 1Nb addition in alloy B seems to improve the protective effect, resulting in very smooth oxidation curves, and very slow oxidation kinetics compared to Type 310 austenitic stainless steel. Alloy C, with additions of 2Nb, showed relatively higher mass gain than alloy B, although the oxidation kinetics were slow and stable similar to the 1Nb-containing alloy. It was found that the addition of 0.1Zr (alloys BZ and CZ) did not significantly impact the oxidation resistance in the current study.

The ash-corrosion tests indicated a beneficial effect of the combined Al + Nb additions on the alloy in the corrosive environment at 700°C, as shown in Fig. 3. The reference binary Fe-30Cr alloy showed very little metal loss with almost no changes in the cross-sectional view, as expected [15], and alloy C with 3Al and 2Nb additions showed only a small amount of metal loss similar to the binary alloy. On the other hand, the alloys with 0Nb (alloy A) or less Al (alloys D and E) showed a significant metal loss with morphology changes in the cross-sectional view. The addition of Zr (alloy CZ) caused a small degradation of corrosion resistance compared to 0Zr alloy (alloy C). The improvement mechanism of corrosion resistance with the Al + Nb additions is not clear yet and detailed characterization is currently in progress.

Figure 4 illustrates the creep-rupture curves at 700ºC and 70MPa of the Fe-30Cr-3Al base alloys, which clearly demonstrate that the creep-rupture life increases with increasing the Nb additions. Almost no creep deformation resistance was observed in alloy A with 0Nb (rupture life: 1.5h), whereas the addition of 1Nb (alloy B) achieved two orders of magnitude longer creep life (134 or 241h) than the 0Nb alloy. The rupture life was further improved by addition of 2Nb (alloy C, ~1,762h) which resulted in longer rupture life than that of Grade 92 steel (~1,188h) at the test condition. It was also found that the effect of grain size on creep rupture life was not significant when compared to that of the Nb additions. The thermodynamic calculation indicated that increased Nb additions result in a greater volume fraction of Laves phases at 700°C. Thus, the test results suggested the importance of the second-phase strengthening optimization, and the volume fraction would be one of the important factors.

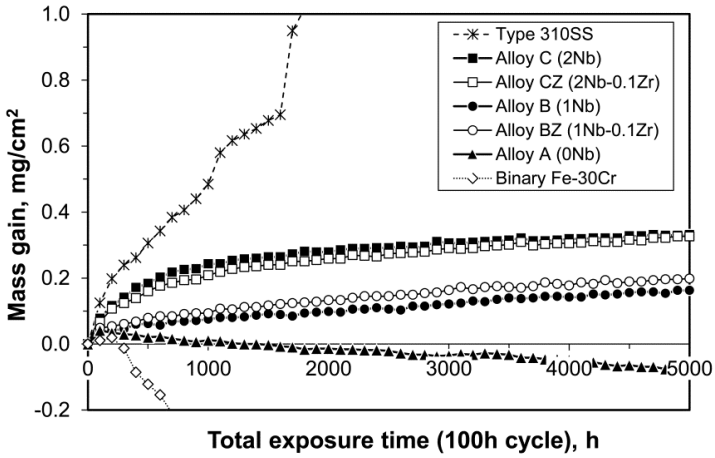

Figure 2: Cyclic oxidation test results at 800ºC in 10% water vapor of Fe-30Cr-3Al base alloys, compared with 310 austenitic stainless steel and binary Fe-30Cr alloy as references.

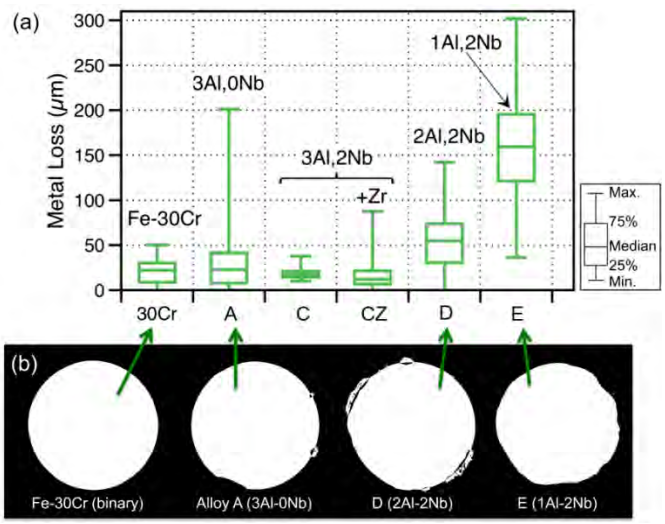

Figure 3: Ash corrosion test result at 700°C for 500h: (a) the metal loss distributions of the alloys tested, and (b) the cross-sectional views of the specimens after testing.

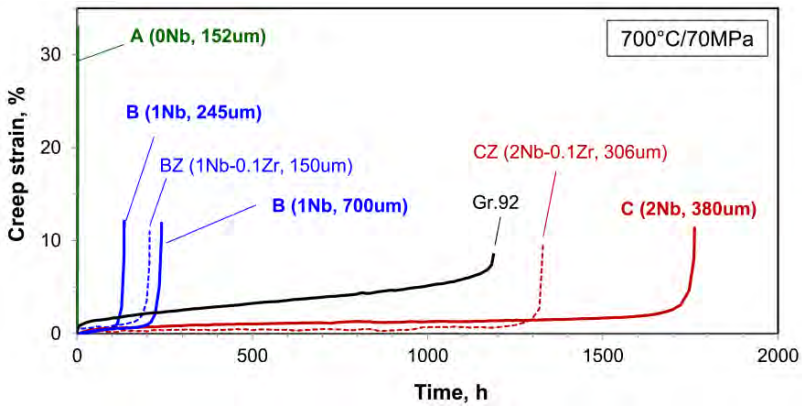

Figure 4: Creep-rupture curves at 700ºC and 70MPa of Fe-30Cr-3Al-0.2Si-(0-2)Nb-(0-0.1)Zr alloys, together with that of Gr 92 (9Cr-2W) ferritic-martensitic steel as a reference. Number in each alloy name corresponds to the grain size of the tested specimen.

Microstructure Characterization of Creep-ruptured Specimens

Figure 5 shows SEM back scattered electron (BSE) images of alloys B and C after creep-rupture testing at 700°C and 70MPa. They were recorded from the gage portion (5a and 5c) or near fracture surface (5b and 5d). They showed Laves-phase precipitates (bright contrast) dispersed inside the grains and formed on the grain boundary. Alloy B showed a finer and denser particle distribution compared to alloy C, although it would not reflect the effect of Nb content directly on the microstructure because of the difference of their creep-lives. However, both exhibited the precipitate denuded zone formed along the grain boundary. Significant amounts of creep voids were observed along the grain boundary near the fracture surface (5c and 5d), indicating that accumulation of creep deformation at the precipitate denuded zone is important to creep deformation of the present alloys.

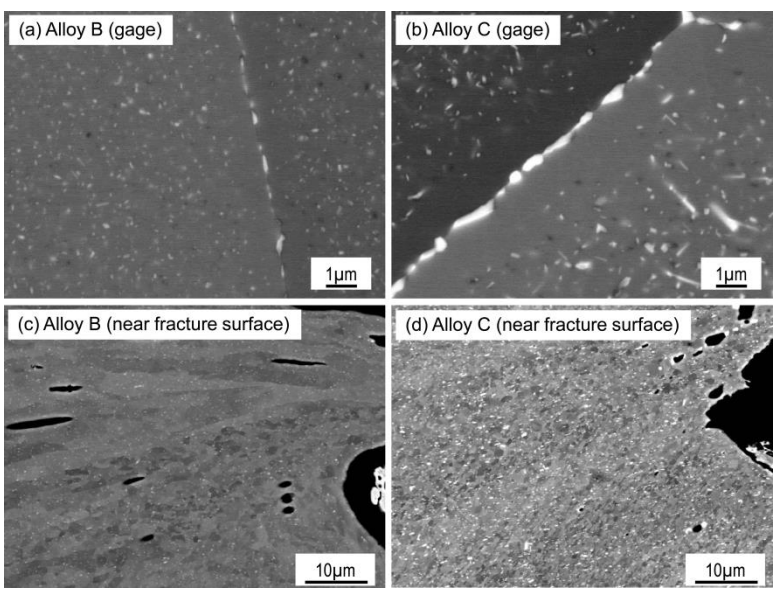

Figure 5: SEM-BSE images of creep-rupture samples tested at 700C and 70MPa; (a) alloy B, and (b) alloy C. The loading direction is parallel to the horizontal axis.

TEM bright field images (BFIs) at the gage portion of alloy C after creep testing indicated a fine dispersion of granular Laves phase precipitates with size typically less than 1μm (Fig. 6a), while the density of the particles was quite lower near grain boundary than the grain interior (Fig. 6b). It should be noted that the dislocations were pinned by the particles inside the matrix, whereas those in the precipitate denuded zone were piled up at the grain boundary precipitates. Therefore, at the current test condition, the creep deformation is concentrated at the precipitate denuded zone which led to void formation along the grain boundary, resulting in creep-rupture along the grain boundary (Fig. 6c).

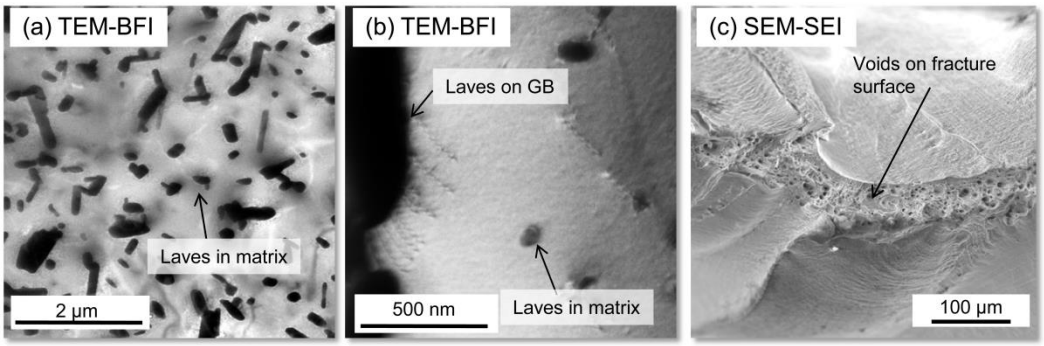

Figure 6: TEM-BFIs of (a) grain interior and (b) grain boundary precipitates, and SEM-secondary electron image of fracture surface of alloy C (2Nb) tested at 700°C and 70MPa.

Effect of Third Alloying Additions

Thermodynamic calculations predicted that third element additions, such as W, Mo, and Ti, would lower the solvus temperature (a full dissolution temperature of Fe_2Nb Laves phase into the bcc-Fe matrix) without reducing the amount of Laves phase at 700°C. As shown in Fig. 4, a large amount of Laves phase formation would be one of the important factors for improving the creep properties. At the same time, the lower solvus temperature would be beneficial for extending the process temperature window without the Laves phase formation. Table 2 summarizes the calculated solvus temperature and the mole fraction of Laves phase at 700°C. Additions of W, Mo, and Ti to the 1Nb alloy increase the amount of Laves phase equivalent to alloy C (2Nb), while the solvus temperatures are ~100°C lower than the 2Nb alloy. Fig. 7 shows the microstructure of alloy C and alloy BW (1Nb-2W) annealed at 1200°C. Alloy C exhibited numerous Laves phase formation, indicating that the calculation underestimated the solvus temperature. However, alloy BW successfully achieved fully solution treated microstructure at the same annealing temperature. Similar microstructure was observed in alloys BM (1Nb-1.5Mo) and BT (1Nb-1Ti) after annealing at 1200°C, suggesting a successful control of the solvus temperatures through the proper alloying additions.

Table 2: Calculated solvus temperature and mole fraction of Laves-phase at 700°C

Alloy	Nominal	Solvus temperature, °C	Mole fraction of Laves phase at 700°C
B	1Nb	994	1.51
C	2Nb (1Nb-1Nb)	1148	3.27
BW	1Nb-2W	1034	2.75
BM	1Nb-1.5Mo	1051	3.34
BT	1Nb-1Ti	1047	3.90

It was also found that the third element additions did not stabilize the particle size at 700°C. Aged microstructures of alloy BW at 700°C (Fig. 8) exhibited fine and dense dispersion of Laves phase precipitates after 168h aging (8a). The particles were coarsened at both grain interior and grain

boundary after 3000h aging (8b), and the particle denuded zone was also observed along the grain boundary. The transgranular particle size was measured from the SEM images, and the size distributions were plotted as cumulative relative fraction curves (Fig. 9a) to define the mean particle size. The mean particle size of the alloys plotted as a function of aging time demonstrated that the additions of W and Mo refined the particle size in the early stage of aging, while the coarsening rates were larger than that of alloy C (9b). It should be noted that they showed similar width of the particle denuded zone after 3000h aging. The Ti additions, on the other hand, showed coarser particle size than alloy C in the range of aging time studied, whereas the coarsening rage was the lowest among the alloys. It was found that the particle denuded zone was the narrowest among the alloys studied.

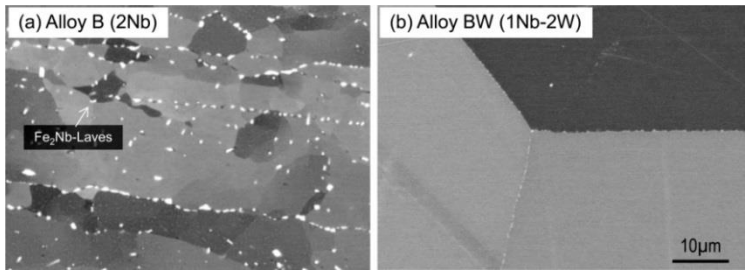

Figure 7: SEM-BSE images of (a) alloy B and (b) alloy BW after annealing at 1200°C.

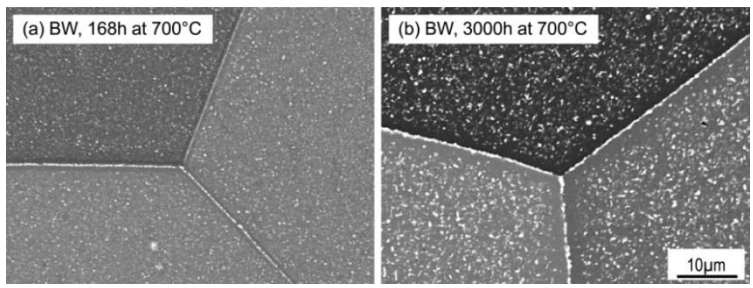

Figure 8: SEM-BSE images of alloy BW after aging at 700°C for (a) 168h and (b) 3000h.

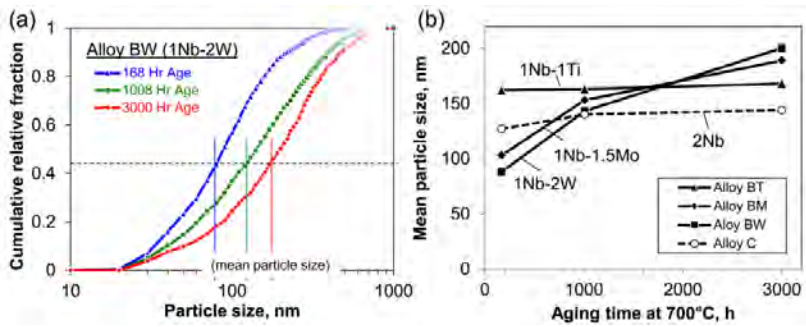

Figure 9: (a) Size distribution of Laves phase precipitates in Alloy BW (1Nb-2W) aged at 700°C for various periods of aging time plotted as cumulative relative fraction curves, and (b) the mean particle sizes of various alloys plotted as a function of aging time.

These results suggest two different approaches for improving creep performance of Nb-containing FeCrAl alloys; (1) eliminating or minimizing the addition of third element (W, Mo, and Ti) for better size stability of Laves phase particles, and (2) optimizing the Ti addition to control the precipitate denuded zone and the particle coarsening kinetics. Further detailed analysis and modification of alloy compositions are currently in progress.

CONCLUSIONS

The effect of minor alloying additions on the properties of newly developed Fe-30Cr-3Al-Nb-Si alloys was investigated. The alloys with more than 1 wt.% Nb addition exhibited improved tensile properties compared to Grade 91/92 steels in a temperature range from 600-800°C, and excellent steam oxidation at 800°C as well. Creep-rupture properties of the 2Nb-containing alloys at 700°C were comparable to Gr 92 steel. The combined addition of Al and Nb was also found to improve ash-corrosion resistance at 700°C, although the mechanism was unclear. Additions of W and Mo were found to refine the Laves phase particles but also promoted the coarsening of the particle size during aging at 700°C, whereas the Ti addition was found to reduce the precipitate denuded zone along the grain boundary and the precipitate coarsening kinetics. Optimization of minor alloying to further improve the creep-rupture performance is currently in progress.

ACKNOWLEDGEMENTS

The authors thank Drs. Dean Pierce, Mike Brady, George Ulrich, and Pete Tortorelli at Oak Ridge National Laboratory for their comments on this manuscript and support of alloy designs in the present study. Research sponsored by the Crosscutting Research Program, Office of Fossil Energy, U.S. Department of Energy.

REFERENCES

[1] Cole, D. G., "Design of Heat-Resistant Steels for Small Power Plant," Doctoral Dissertation, University of Cambridge, UK, 2000.
[2] Abe, F., *Science and Technology of Advanced Materials*, v. 9, p. 013002, 2008.
[3] Shibli, I. A., *OMMI*, v.1, no. 3, pp. 1-17, 2002.
[4] Henry, J. F., *Combined Cycle Journal*, First Quarter, p. 8, 2005.
[5] Shibli, I. A. and Coleman,K., (www.ommi.co.uk/ etd/ETD-EPRI-%20P91%20Failures.pdf)
[6] Berte, F. J., *Combined Cycle Journal*, Second Quarter , p. 52, 2007.
[7] Francis, J. A., Mazur, W. and Bhadeshia, H. K. D. H., Mater. *Sci and Technol*., v. 22, p. 1387, 2006.
[8] Abe, F. and Tabuchi, M., *Mater Sci and Technol*., v. 9, p. 22, 2004.
[9] Hirata, H. and Ogawa ,K., *Weld. Int*, v. 19, p. 37, 2005.
[10] Yu, X., Babu, S. S., Terasaki, H., Komizo, Y., Yamamoto, Y. and Santella, M. L., *Acta Materialia*, v. 61, pp. 2194-2206, 2013.
[11] Toda, Y., Auchi, M., Sawada, M. K., Kushima, H., Kimura, K., *Proceedings of the 10th Liège Conference: Materials for Advanced Power Engineering 2014*, B. Kuhn *et al* (Eds.), September 2014; pp. 239-247.
[12] Kuhn B., and Talik, M., *Proceedings of the 10th Liège Conference: Materials for Advanced Power Engineering 2014*, B. Kuhn *et al* (Eds.), September 2014; pp. 264-273.
[13] Yamamoto, Y, Babu, S.S., Shassere, B., Yu, X., "Performance Improvement of Creep-Resistant Ferritic Steel Weldments through Thermo-Mechanical Treatment and Alloy Design" in *Proceedings of the 1st international conference on Advanced High-Temperature Materials Technology for Sustainable and Reliable Power Engineering (123HiMAT-2015)* (June 29 - July 3, 2015, Sapporo, Japan), the 123rd Committee on Heat Resisting Materials and Alloys, Japan Society for the Promotion of Science, pp.66-69 (2015).
[14] Yamamoto, Y., Brady, M.P., Santella, M.L., Bei, H., Maziasz, P.J. and Pint, B.A.: *Metall Mater Trans A*, 42A (2011) pp. 922-931.
[15] Pint, B.A. Thomson, J.K.,: *Materials and Corrosion*, 65, 2 (2014) pp. 132-140.